Krzysztof HOLAK*, Piotr KOHUT*, Adam MARTOWICZ*, Tadeusz UHL*

AN UNCERTAINTY ANALYSIS FOR DEVELOPED MEASUREMENT VISION SYSTEM AIDED BY NUMERICAL SIMULATIONS

SUMMARY

The paper presents an optical non-contact method of measuring the static deflection structure in one plane. Displacements of measurement points of the structure under the load were computed by means of digital image correlation coefficient. The application of homography mapping enabled the deflection field to be computed from two images of the structure acquired from two distinct points in space. The model of the developed vision system were implemented and simulated in the MATLAB programming tool. The impact of the corner detector inaccuracy on the measurement results was investigated. The uncertainty propagation of the developed method was examined in a series of simulations. The distance of the camera and the focal length were investigated parameters of the system. In the paper, the variability of homography components as well as variability of displacements measured in each of the points of interest are presented.

Keywords*: digital image correlation, homography transformation, vision system, deflection measurement*

ANALIZA NIEPEWNOŚCI POMIAROWEGO SYSTEMU WIZYJNEGO WSPOMAGANA EKSPERYMENTEM NUMERYCZNYM

W artykule zaprezentowano optyczną bezkontaktową metodę pomiarową ugięć statycznych konstrukcji w jednej płaszczyźnie. Przemieszczenia punktów pomiarowych obiektu będącego pod działaniem obciążeń zostały wyznaczone za pomocą znormalizowanego współczynnika korelacji. Zastosowanie przekształcenia homograficznego umożliwiło uzyskanie krzywej ugięcia konstrukcji na podstawie dwóch obrazów wykonanych z dwóch różnych punktów przestrzeni. Numeryczny model wizyjnego systemu pomiarowego został zaimplementowany w środowisku MATLAB. W pracy zbadano wpływ niedokładności detektora narożników Harrisa na wynik pomiarów. Propagacja niepewności opracowanej metody pomiarowej została wyznaczona w serii eksperymentów symulacyjnych. Badanymi parametrami systemu były: odległość kamery od obiektu oraz ogniskowa. W artykule przedstawiono zmienność elementów macierzy homografii oraz wartości przemieszczeń wyznaczanych przez system w każdym z punktów pomiarowych.

Słowa kluczowe*: korelacja obrazów cyfrowych, przekształcenie homograficzne, systemy wizyjne, pomiary odkształceń*

1. INTRODUCTION

Vision-based techniques belong to the group of non-contact global Structural Health Monitoring methods which enable global measurements of static deformations to be carried out. Their main advantages are: high measurement density, low cost and universality. In the diagnostics of civil engineering structures, measurements of displacements are the major tool of the static states evaluation. They allow damage detection to be performed by means of an analysis of a change in the geometry of a structure.

The nature of real measurements features immanent uncertainty (Bornert *et al*. 2009, De Santo *et al*. 2004). Limited quality of measurement equipment inevitably results in the variation of yielded outcomes. Therefore it seems justified the utilization of both the sensitivity analysis and the assessment of uncertainty propagation (Moens *at al*. 2006, Schueller 2006). They can be performed to check the quality of optical tools applied in the area of SHM (Giurgiutiu 2008, Park *et al*. 2007). A deterministic assessment introduces no information how the measured response varies in the presence of identified uncertainties. The solution that helps to overcome mentioned inconvenience could be a series of measurements performed in order to determine required statistics and scatters. Stochastic analyses allow to search for the relationships between interesting input and output parameters as well as to find the best configuration of measurement equipment which characterizes the least sensitivity to present uncertainty.

Identified uncertainties can be modeled as random numbers or fields, intervals or fuzzy numbers (Moens *at al*. 2005, Schueller 2006). In case of random numbers they are represented with statistics of chosen orders, e.g. mean, standard deviation, etc, or probability density functions (PDF). Random fields stand for an extension of random numbers since they are used spatial PDF with assumed correlation between input characteristics e.g. defined with the correlation length (Schueller 1997).The random fields can be successfully applied for instance for modeling the roughness of a surface. An applied form of uncertainty modeling determines the method which can be used for the uncertainty and sensitivity analyses. There are distinguished probabilistic

* AGH University of Science and Technology, Faculty of Mechanical Engineering and Robotics, Department of Robotics and Mechatronics, al. A. Mickiewicza 30, 30-059 Krakow, Poland; holak@agh.edu.pl, pko@agh.edu.pl, martowicz.adam@agh.edu.pl, tuhl@agh.edu.pl

and possibilistic computational techniques. The first group can deal with random numbers and fields. The Monte Carlo simulation (MCS) is commonly applied to find PDF and statistics (Schueller 1997). The latter group in turn can be used in case of intervals and fuzzy numbers (Moens *at al*. 2005, Dubois 1980, Moore 1966).

The most known computational methods are: the interval analysis, the vertex method, fuzzy sets theory including the Zadeh's extension principle and the transformation method with their several improvements (Donders *et al*. 2005, Hanss 2002, 2005). As the alternative to the fuzzy number theory and the transformation method the application of the effective alpha-cut strategy can be also considered (Donders *et al*. 2005). Uncertainty analyses make the results of numerical simulations be closer to real experiments. They also help to understand true nature of a phenomena present in mechanical structures while their operation. The sensitivity analysis may help to exclude those input parameters which are noninfluential.

2. VISION IN-PLANE DEFLECTION MEASUREMENT METHOD

The developed vision in-plane deflection measurement method consists of the following steps calibration, rectification and deflection measurement (Uhl *et al*. 2009, 2009a): In the first step, the calibration of the system is performed. The scale coefficient is calculated from objects on the scene with known geometric dimensions (calibration disks with known diameter, calibration squares, length standards). The method provides the full calibration of intrinsic and extrinsic camera parameters with the third degree model of lens distortions. Lens distortions reduction is an optional step of the method. The reference image and two or more images of the construction under the load are acquired by the camera. The successive photographs can be taken from distinct points in space. The second step is the automatic detection and matching of markers coplanar with the plane of the measured construction and the calculation of the homography matrix **H**. The mapping **H** is applied to all the photographs in order to remove the projective distortions from an image of one, particular plane of the structure, which makes it possible to spatially overlay photographs acquired from different points in the space with the reference image. In the third step, the image of the construction is divided into parts – intensity patterns and then positions of the corresponding patterns on the reference image and images of the structure under the load are found by means of the normalized cross correlation coefficient (NCC). The deflection curve is computed from the data obtained in that step. The sub-pixel techniques are introduced to increase the accuracy of the displacement measurement. In the last step, the scale coefficient is applied to rescale the beam's deflection curve to metric units. An interpolation of the scale coefficient value in every measurement points is possible if at least two calibration pattern are attached to different parts of the construction (Uhl *et al*. 2009, 2009a) The method is schematically described in the Figure 1.

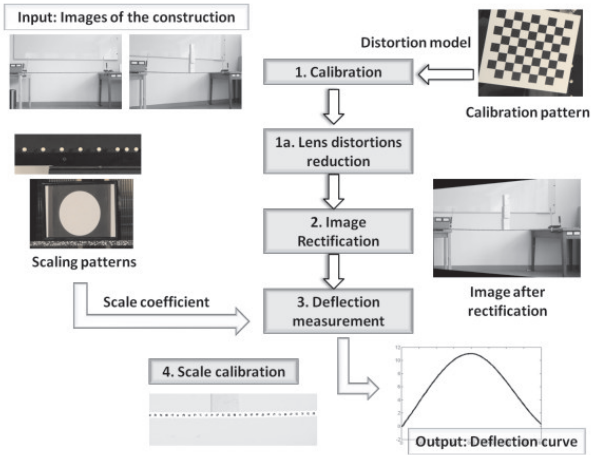

Fig. 1. Main steps of the developed algorithm

Calibration of the system

The full calibration (Ma *et al*. 2004) of the vision system is carried out in order to obtain the intrinsic calibration matrix **K** and the set of four radial and tangential lens distortions coefficients. The calibration is performed by means of Zhang method (Ma *et al*. 2004, Hartley *et al*. 2004). The chessboard planar pattern with black and white squares, an even number of rows and odd number of columns is used. The scale coefficient $\alpha_{mm/pix}$ is computed from an object on the scene with known geometric dimensions.

Rectangle detection algorithm

In the next step of the method, the boundaries enclosing all foreground objects are detected automatically. The boundaries are filtered by the shape filter whose response is the strongest for convex, rectangular contours with an user defined ranges of area, width to height ratio and angle between adjoining sides of the quadrilaterals. The method is illustrated in Figure 2. Positions of corresponding vertices

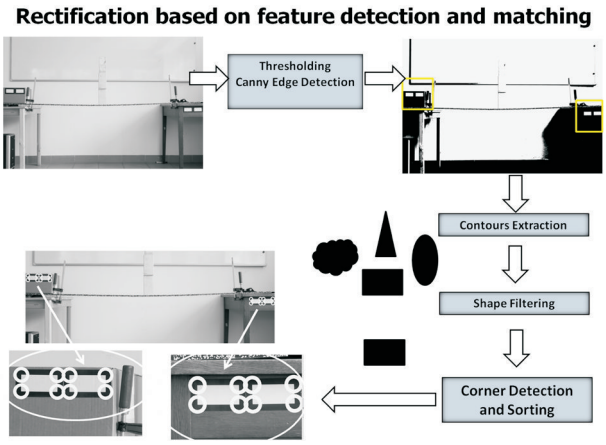

Fig. 2. Rectangle detection algorithm carried out on lab set-up image

of markers at both images are refined by the Harris corner detector (Ma *et al*. 2004). Each of the corners of the rectangular contours found by the shape filter is located automatically by the sub-pixel corner detector. The point at the close neighborhood of the rectangle's vertex with the highest response rate of the Harris detector is taken as a new, refined approximation of the position of the real boundary vertex.

Planar homography transformation

The homography (Harltley *et al*. 2004, Zitova *et al*. 2003) is a mapping which transforms a set of points on the plane into different set of points on the same plane and is denoted by matrix **H**. If the corresponding points are represented in homogenous coordinates as vectors **x** and **x'**, the transformation which maps coplanar points of the image with projective distortions to corresponding points of the reference image is given by the equation:

$$x = Hx' \tag{1}$$

Where **H** is the homography transformation matrix:

$$\mathbf{H} = \begin{bmatrix} h_{11} & h_{12} & h_{13} \\ h_{21} & h_{22} & h_{23} \\ h_{31} & h_{32} & h_{33} \end{bmatrix} \tag{2}$$

In equation (2) the matrix elements h_{13} and h_{23} represent the translation. The elements of the upper left 2×2 sub-matrix are associated with the rotation, shear transformation and scaling. The last row of the matrix **H** is responsible for the perspective and non uniform foreshortenings. The last element h_{33} of the normalized form of the homography matrix is always equal to 1.

The homography matrix **H** is computed from a set of at least four coplanar corresponding points by the linear least squares algorithm (DLT) (Hartley *et al*. 2004). The image of the construction is rectified if all its pixels are transformed by the homography mapping. The results of the rectification algorithm at the real image are shown in Figure 3.

Deflection measurement by the means of the normalized correlation coefficient

The value of the digital image correlation coefficient (Chu *et al*. 1985) calculated at the pixel of the image is equal to the degree of similarity between the region centered on that pixel and a given intensity template. The normalized cross correlation coefficient can reach values from interval [–1, 1]. When values of an analyzed region of the image are the same as values of the intensity from the known intensity pattern, the correlation coefficient is the maximum and is equal to 1. The cross correlation coefficient (NCC) is used for the computation of the displacement field. The reference image of the unloaded construction is divided into intensity patterns (Uhl *et al*. 2009, 2009a). Positions of each of the intensity patterns are calculated for both of images: the reference one and the rectified one by means of the correlation coefficient. In the developed method, only the local search in the neighborhood of each intensity pattern is performed. Displacement vector for each of the measurement points is computed as a difference between positions of the pattern on two images of the construction: taken before and after deformation (Fig. 4). Calculation carried out on each of the points of interest gives complete course of deflection. The correlation method was refined by a sub-pixel technique which made it possible to increase the measurement accuracy up to 0.01–0.1 parts of a pixel.

Fig. 3. The reference image (a) the image captured from a different point in space (b) the image rectified by the homography matrix (c)

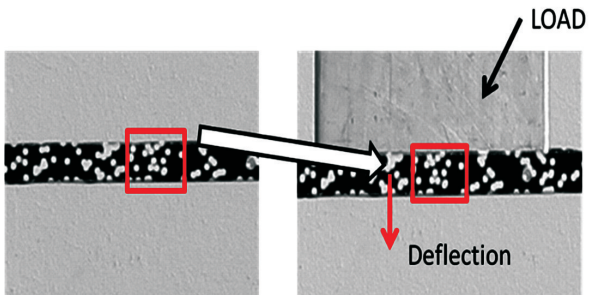

Fig. 4. The same intensity pattern found on the reference image the image of the construction under the load

3. NUMERICAL SIMULATION OF THE METHOD

In order to carry out the uncertainty analysis of the method, the discrete model of the scene consisting of the virtual camera and the construction were developed in MATLAB programming tool. The model consists of the pinhole camera with the known internal (f_{sx}, f_{sy}, u_0, v_0, s_θ) and external (**R, T**) calibration matrices (Ma *et al.* 2004), its projection model given by equation (3) and the virtual image plane.

$$\lambda\begin{bmatrix} u \\ v \\ 1 \end{bmatrix} = \begin{bmatrix} fs_x & s_\theta & u_0 \\ 0 & fs_y & v_0 \\ 0 & 0 & 1 \end{bmatrix}\begin{bmatrix} f & 0 & 0 \\ 0 & f & 0 \\ 0 & 0 & 1 \end{bmatrix}\begin{bmatrix} 1 & 0 & 0 & 0 \\ 0 & 1 & 0 & 0 \\ 0 & 0 & 1 & 0 \end{bmatrix}\begin{bmatrix} \mathbf{R} & \mathbf{T} \\ \mathbf{0} & 1 \end{bmatrix}\begin{bmatrix} X \\ Y \\ Z \\ 1 \end{bmatrix} \quad (3)$$

Table 1

The focal lengths used in simulations with the associated reference distances to the construction

Focal length f [mm]	Reference distance d_0 [mm]
12	500
35	1200
50	1800
80	2500

The virtual camera with 21.1 Mega pixel resolution sensor and the lens with adjustable 4 different focal lengths (f = 12 mm, 35 mm, 50 mm and 80 mm) were modeled. For each of the focal lengths there were associated reference distances between the camera and the construction. They were summarized in the Table 1. The model of construction consisted of a simply supported beam loaded by a point force acting centrally and a set of markers coplanar with the beam's plane needed for the image rectification. The FEM model of the beam was constructed in MATLAB from 1D beam elements. The steel beam of length 800 mm, cross section area 500 mm^2 and elastic modulus equal to $2.1\cdot10^5$ MPa was modeled. The construction was loaded by a point force of magnitude 1000 N. The set consisting of 6 markers was positioned symmetrically with respect to the structure (Fig. 5). In the analysis of the variability of the method, the homography matrix components and calculated deflection of the beam were taken as tested parameters.

In the simulations, the uncertainty is considered for all the corner coordinates of used 6 markers. A random noise described by normal probability distribution function is added to the nominal values of both vertical and horizontal coordinates of the corner points.

In the next discussion, the following notation, concerning the simulation experiment, will be used: each of the measurement series will be designated as fXdY, where X – the focal length value [mm], Y – the reference distance for a given focal length [mm], for example: f50d1800 means the images obtained by a camera with a focal length 50 mm and a reference distance d = 1800 mm.

4. RESULTS OF THE SIMULATIONS

The first analysis deals with the assessment of the uncertainty propagation for the case when the distance d_1 between the camera and observed object is changed within the specified bounds (for example, for a focal length f = 50 mm, from 500 mm up to 7500 mm). In all the figures, the relative distance (a distance increase) with respect to the reference, denoted as d_0, is presented. For each displacement of the camera, there are assumed several standard deviations attached to the localizations of marker corners, i.e.: 0.005, 0.05, 0.5, 1, 1.5, all defined with pixels as units. In the following the variation of the components of rectification matrix is discussed. Figures 6a and b present the standard deviations and mean values of all matrix components obtained for an exemplary case with the input standard deviations 0.5 pixels and for the reference distance equal to 1500 mm between the camera and object.

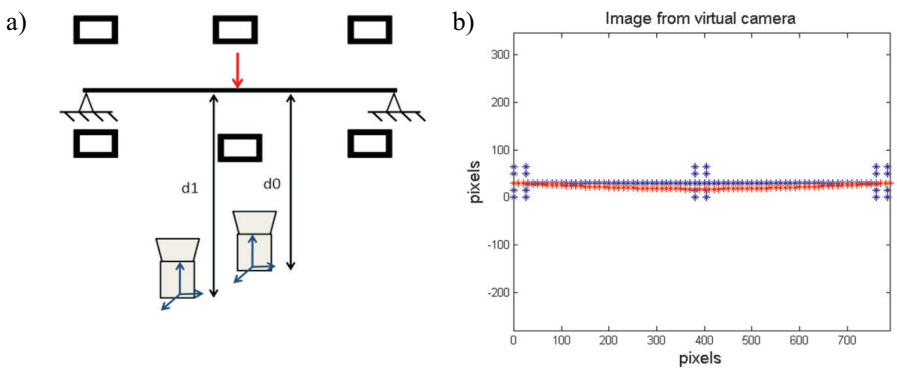

Fig. 5. The camera setup modeled in the simulations: two pinhole projection cameras at the distance d_0 (reference) and d_1 from the construction (a) the virtual image plane with the image of the construction (b)

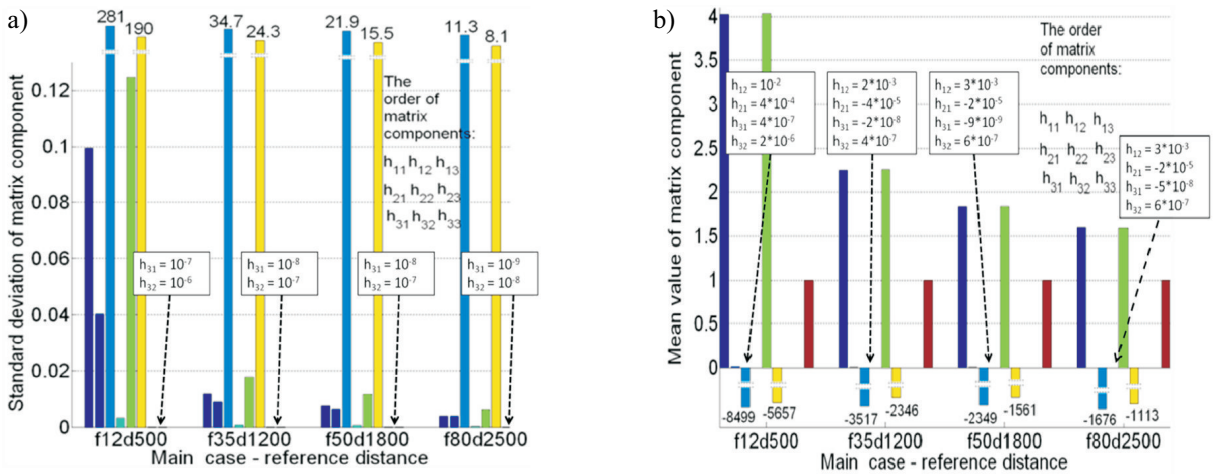

Fig. 6. Standard deviation of matrix components for a chosen input standard deviation equal to 0.5 pixels (a) mean value of matrix components for a chosen input standard deviation (b)

The variation of the first chosen component of the rectification matrix h_{11} for different input standard deviations is shown in Figure 7a. In the experiment, the reference distance equal to 1200 mm with the focal length equal to 35 mm were assumed. There should be noted a nonlinear relationships between the distance to object increase and the resultant standard deviation of the corresponding matrix component. The same observation relates to the remaining matrix components excluding h_{33} which is normalized to unity in all cases. Figure 7b shows the variation of chosen matrix component h_{11} for all reference cases and the chosen distance from the camera to the object equal to 1500 mm. Figure 8 enables for the comparison of components of the rectification matrix for the case when the reference distance is equal to 1200 mm and the focal length is equal to 35 mm.

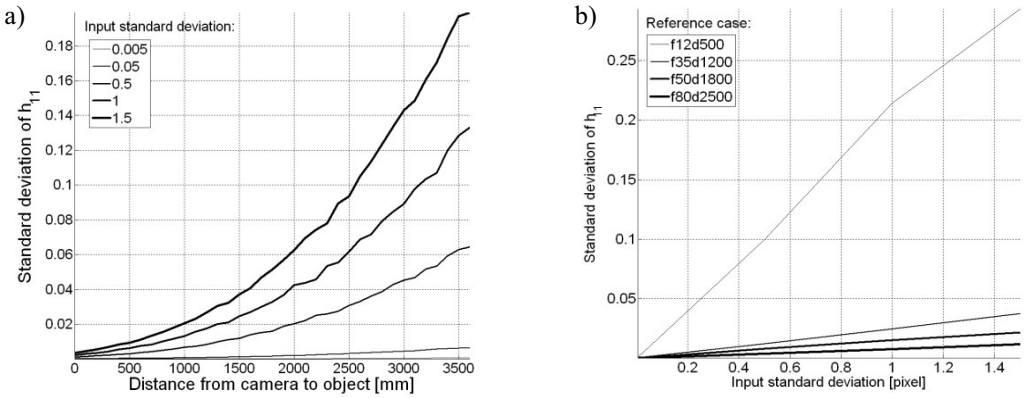

Fig. 7. Standard deviation of the matrix component h_{11} for the chosen reference case (a) Standard deviation of the matrix component h_{11} for the chosen distance to the object (b)

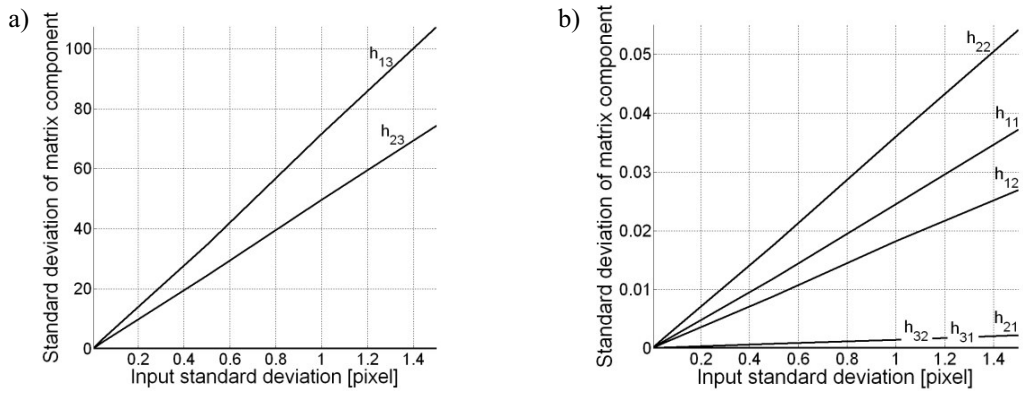

Fig. 8. Standard deviation of all components of the rectification matrix for the chosen reference case (a) the components h_{13}, h_{23}, the remaining matrix components (b)

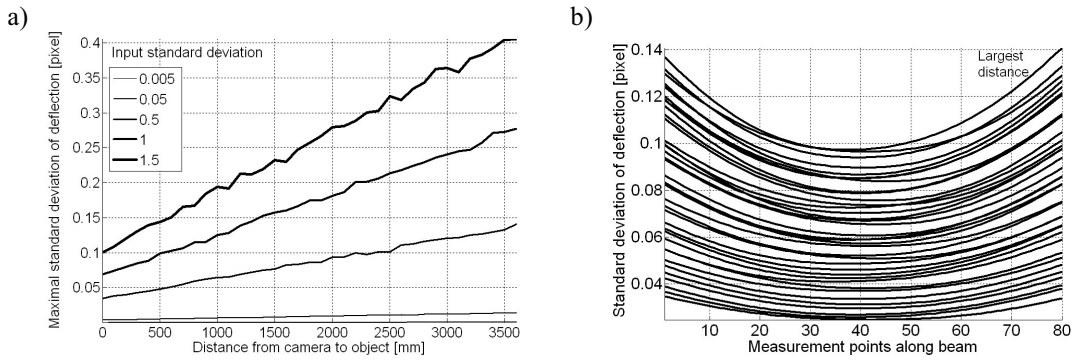

Fig. 9. Maximal standard deviation of static deflection for the reference case (a) standard deviation of static deflection measured along the beam (b)

Figure 9a presents the maximal standard deviation of the static deflection of studied beam found for all measurement points for chosen referential case with the distance 1200 mm and with the focal length 35 mm. Irrespectively to small fluctuations observed for plotted curves there are found linear relationships between input and output standard deviations. Figure 9b shows an exemplary group of curves found for all measurement points localized along the beam and defining the standard deviation of the static deformation for an exemplary case with the input standard deviations 0.5 pixels. As expected the best accuracy can be achieved in the middle of the beam. The curves with the smallest values of standard deviations are related to the smallest distances to the camera. However the ratio between these parameters measured for both the worst and the best case along the beam decreases when increasing the distance.

The next analysis deals with the assessment of the uncertainty propagation for different focal lengths being taken from the interval: 12 mm up to 80 mm. Again, there are assumed different standard deviations attached to the localizations of marker corners: from 0.005 up to 1.5 pixels. In the following, at first, the variation of the components of the rectification matrix is discussed. Figure 10 presents the standard deviations and mean values of all matrix components obtained for the experimental case when the input standard deviations is equal to 0.5 pixels and the focal length is equal to 52 mm.

In Figure 11a there is shown the variation of the first component of the rectification matrix h_{11} for different values of input standard deviations for the exemplary case of the reference distance 1200 mm and with the focal length 35 mm. Nonlinear relationships for all matrix components are observed, again excluding h_{33}. Figure 11b shows an exemplary group of curves found for all measurement points localized along the beam and defining the standard deviation of the static deformation for an exemplary case with the input standard deviations 0.5 pixels. As expected the best accuracy can be achieved in the middle of the beam. The curves with the smallest values of standard deviations are related to the greatest focal length. The ratio between these parameters measured for both the worst and the best case along the beam decreases as the focal length decreases too.

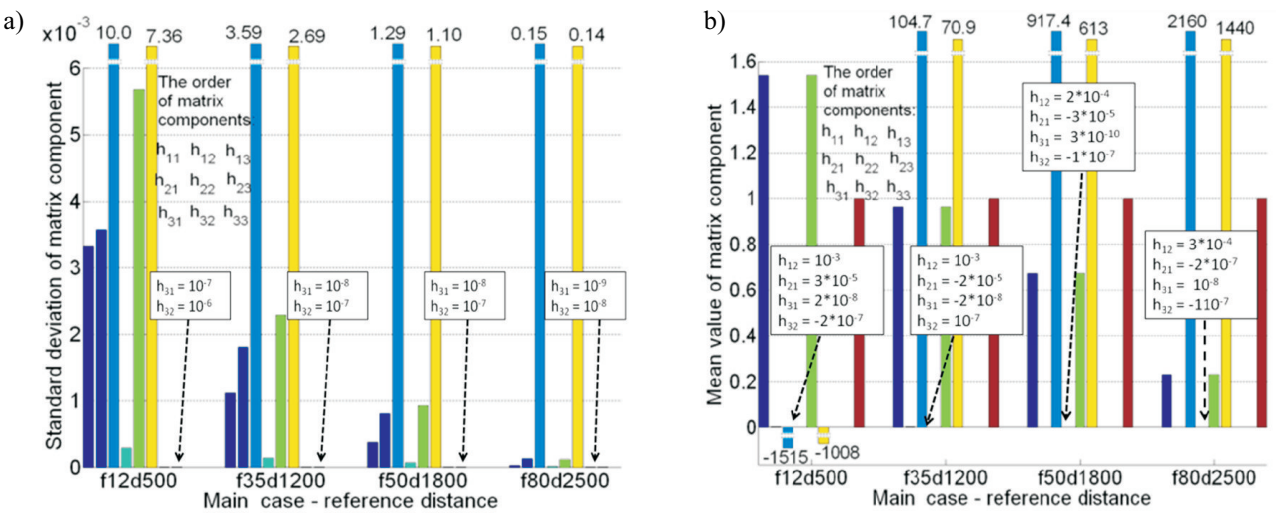

Fig. 10. Standard deviation of matrix components for a chosen input standard deviation equal to 0.5 pixels (a) mean value of matrix components for a chosen input standard deviation (b)

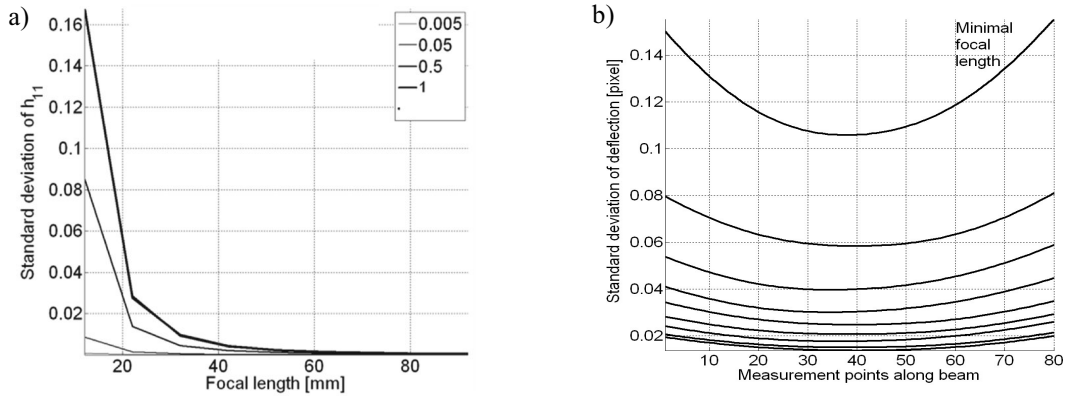

Fig. 11. Standard deviation of the h_{11} homography matrix element for different standard deviations of the noise(a) standard deviation of the static deflection measured along the beam (b)

5. CONCLUSIONS

The experiments revealed that the h_{13} and h_{23} components associated with the translation part of the homography matrix characterize the largest sensitivity to inaccuracies of the corner detector. However, the mean values of these parameters have been much larger than the remaining components of the matrix **H**. As it is expected, the standard deviation of the homography elements associated with the perspective is less than 0.001 in both tested cases. It is consistent with the modeled change of the camera parameters. In the simulation, the virtual camera was undergoing one of two types of its parameters' variation: change of its focal length or change of its distance from the construction. These variations resulted in two types of the virtual image modifications: the change of its size or its translation on the image plane without introducing any perspective foreshortenings. The relationship between the standard deviation value of the input to the algorithm (corners positions) and the standard deviation of the output (the homography components) has been linear in both studied examples. However, the numerical examination has revealed it to be a function of the focal length. The rate of change of the output standard deviation was the highest for the focal length equal to 12 mm (i.e. 0.2 for h_{11} component). The research has exposed that it was an order of magnitude smaller (0.01 for the same matrix element) for the focal lengths greater than 35 mm. The images acquired by a camera with a small focal length exposed the largest perspective distortions, and therefore the scale of the object on the images was not constant along its length. Numerical examination proved that the performance of the rectification algorithm was the worst in this case. The larger focal length can be approximated by a camera with a center at the infinity and therefore the projective distortions are negligible.

The nonlinear relationship between the camera distance to the object and the standard deviation of the matrix **H** elements was observed for all **H** components. It should be noticed that the aforementioned relationship was approximately linear for the reasonable change of the distance for which the image was physically not out of focus (i.e. 1000 mm for f = 35 mm). The strong nonlinear relationship has existed also for the occurrence in which the change of the focal length value has been tested.

Research has showed that the relationship between the camera distance to the object and the maximal value of standard deviation of the beam's deflection has been linear. Another very significant observation has indicated that deflection's standard deviation has turned out to be less than corners positions' standard deviation for all cases of the input noise level. For example, the standard deviation of the input amounts to 1.5 pixels, results in the standard deviation of the output equal to 0.4 pixels. The largest impact of the input's noise has been observed at the end points of the beam. It is reasonable, since there are the smallest displacements of points and their measurement is easily disturbed by the noise in the image. The highest value of deflection's standard deviation was found for the focal length f = 12 mm, irrespective of the chosen point of the measurement. However, the effect of the noise imposed on the corresponding points coordinates was insignificant in all other cases. The maximal standard deviation of the deflection was amounted to 0.15 pixels for the largest inspected distance of the camera, but it was observed that it reached values less than 0.05 pixels for a physically feasible distance to the object. It has exposed significant practical implications. If the scale coefficient was equal to i.e. 0.3 mm/pixel, the uncertainty in the deflection measurement equaled ±0.003 mm ($2\cdot\sigma$) which was acceptable. Research has proved that the homography transformation can be introduced in the vision measurement systems for the image rectification, however the application of small focal lengths hasn't been recommended.

The technique of the in-plane deflection measurement presented in this article enables images of the construction to be taken from different points of view during examination. Simplification of the measurement procedure is possible because the complicated, expensive and time-consuming step of camera positioning is not necessary. The system has provided high measurement density without an use of active optical methods.

References

Bornert M., Brémand F., Doumalin P., Dupré J.-C., Fazzini M., Grédiac M., Hild F., Mistou S., Molimard J., Chu T.C., Ranson W.F., Sutton M.A., Peters W.H., 1985, *Application of digital-image correlation techniques to experimental mechanics*. Exp Mech., 25, pp. 232–24.

De Santo M., Liguori C., Paolillo A., Pietrosanto A., 2004, *Standard uncertainty evaluation in image-based measurements*. vol. 36, Issues 3–4, pp. 347–358.

Donders S., Vandepitte D., Van de Peer J., Desmet W. 2005, *Assessment of uncertainty on structural dynamic responses with the short transformation method*. Journal of Sound and Vibration, vol. 288, pp. 523–549.

Dubois D., Prade H. 1966, *Fuzzy sets and systems. Theory and applications*. Academic Press, New York 1980.

Giurgiutiu V. 2008, *Structural Health Monitoring with Piezoelectric Wafer Active Sensors.* Elsevier Academic Press, Amsterdam, Boston.

Hanss M. 2005, *Applied fuzzy arithmetic. An introduction with engineering applications*. Springer-Verlag, Berlin.

Hanss M. 2002, *The transformation method for the simulation and analysis of systems with uncertain parameters*. Fuzzy Sets and Systems, vol. 130, pp. 277–289.

Hartley R., Zisserman A., 2004, *Multiple View Geometry in Computer Vision*. Cambridge University Press.

Ma Y., Soatto S., Kosetska J., Sastry S. 2004, *An Invitation to 3D Computer Vision*. Springer-Verlag, New York.

Martins J.A.C., Rodrigues H.C., Ambrosio J.A.C. 2006, *Computational Mechanics*. Solids, Structures and Coupled Problems. Springer, Dordrecht, The Netherland, pp. 541–554.

Moens D., Vandepitte D. 2005, *A survey of non-probabilistic uncertainty treatment in finite element analysis*. Computer methods in applied mechanics and engineering, vol. 194, pp. 1527–1555.

Moens D., Vandepitte D. 2006, *Interval sensitivity analysis of dynamic response envelopes for uncertain mechanical structures*. Proc. of III ECCM – European Conference on Computational Mechanics, Lisbon, Portugal, June 5–9.

Moore R.E.: *Interval analysis*. Englewood Cliffs, N.J., Prentice-Hall.

Orteu J.-J. 2009, *Assessment of Digital Image Correlation Measurement Errors: Methodology and Results*. Experimental Mechanics, vol. 49, No. 3, pp. 353–370.

Park G., Inman D.J. 2007, *Structural health monitoring using piezoelectric impedance measurements.* Phil. Trans. R. Soc. A 365, pp. 373–392.

Schueller G.I., *Uncertainty & reliability analysis of structural dynamical systems*. [Eds.] Mota Soares C.A.

Schueller G.I. 1997, *A state-of-the-art report on computational stochastic mechanics*. Probabilistic Engineering Mechanics, vol. 12(4), pp. 197–321.

Uhl T., Kohut P., Szwedo M., Holak K. 2009, *Static and dynamic optical measurement in SHM of civil structures*. Proc. of the 7th international workshop on Structural Health Monitoring, DESTech publications, Lancaster, pp. 1765–1773.

Uhl T., Kohut P., Holak K. 2009a, *Image correlation and homography mapping in optical deflection measurement*. OPTIMESS, Proc. of the 4th international conference on Optical Measurement Techniques for Structures & Systems, 25–26 May Antwerp, Belgium, pp. 191–200.

Zitova B., Flusser J. 2003, *Image registration methods: A survey*. Image and Vision Computing 21, Elsevier.